Article:
Sanchez Segado, S, Lahiri, A and Jha, A (2014) Alkali roasting of bomar ilmenite: rare earths recovery and physico-chemical changes. Open Chemistry, 13 (1). 270 - 278. ISSN: 2391-5420

https://doi.org/10.1515/chem-2015-0033

Invited Paper **Open Access**

Sergio Sanchez-Segado*, Abhishek Lahiri, Animesh Jha

Alkali roasting of bomar ilmenite: rare earths recovery and physico-chemical changes

Abstract: In this work, the alkali roasting of ilmenite ($FeTiO_3$) is presented as a process route for integrated beneficiation of the mineral for rutile-rich phase and rare earth oxides; the latter is released as a consequence of physical changes in the ilmenite matrix, during the water leaching after roasting. The oxidative alkali roasting transforms ilmenite mineral into water-insoluble alkali titanate and water-soluble ferrite. After roasting the insoluble alkali titanate is separated from rare-earth oxide mixture in colloidal form and water-soluble ferrite. Further leaching of alkali titanate is carried out with oxalic (0.3M) and ascorbic (0.01M) acid solution which removes the remaining Fe^{2+} ions into the leachate and allows precipitation of high-purity synthetic rutile containing more than 95% TiO_2. Iron is removed as iron oxalate. The physico-chemical changes occurred during the roasting and leaching processes are reported by comparing the role of alkali on the roasting process and product morphologies formed.

Keywords: Titanium, Rare Earth oxides, Leaching, Selective separation, Synthetic Rutile.

DOI: 10.1515/chem-2015-0033
received February 07, 2014; accepted April 6, 2014.

1 Introduction

Titanium is the ninth most abundant element in the Earth's crust and it can be found in six different minerals as a single or complex oxide (rutile, anatase, brookite, perovskite, ilmenite and leucoxene). Since the oxide market is much larger in size than the pure metal [1], the demand for high-grade TiO_2 is increasing for applications in paints and pigments, paper, plastics, and in welding flux. There is also pressure on aerospace industry to use Ti-alloy components for energy saving. Other emerging applications are in the production of electrochromic devices, gas sensors, hydrogen storage systems and fuel cells [2].

Ilmenite is one of the most common mineral sources used for the extraction of synthetic rutile. The ilmenite production in 2011 in each continent is shown in Fig. 1 [3], with the American continent being the largest source of this mineral.

To understand the production of titanium dioxide (synthetic rutile) from ilmenite, it is necessary to analyze the crystal structure. Ilmenite has some similarity with the normal spinel structure, which is cubic in contrast with the hexagonal structure of ilmenite, as shown in Fig. 2.

In Fig. 2, Fe^{2+} is tetrahedrally coordinated whereas Ti^{4+} adopts its energetically favourable octahedral coordination, forming alternate layers inside an oxygen anion sub lattice. In this alternate structure there is competition for site occupancy, especially the transition element cations Fe^{3+}, Cr^{3+}, Mn^{3+} via octahedral site substitution, whereas the divalent ions such as Mg^{2+}, Ca^{2+} may replace Fe^{2+}, depending on other cations at octahedron sites. The net charge balance is 3+ per anion in the structure [4]. Other significant mineralogical factors to take into consideration for ilmenite minerals is the presence as exolved phases of zircon ($ZrSiO_4$) and monazite $(Al,RE)PO_4$ which are finely distributed within the ilmenite matrix, and make their physical separation extremely difficult [5]. The presence of zircon and monazite degrade the mineralogical value of ilmenite for synthetic rutile production, which is why the ilmenite deposits with higher concentrations of exsolved zircon and monazite are undesirable for mineral beneficiation.

Foley *et al.* [6] investigated the roasting of low grade ilmenite with Na and K carbonates and found the formation of several (Na or K)-Fe-Ti oxides and Fe_2O_3 as exolved phase. It was also reported that the leaching of (Na or K)-Fe-Ti oxides with HCl 20% solution for iron removal was higher compared to using potassium salts. Subsequently, comparable observations were reported by

***Corresponding author: Sergio Sanchez-Segado:** Institute for Materials Research, Houldsworth Building, University of Leeds, Leeds LS2 9JT, UK, E-mail address: s.sanchezsegado@leeds.ac.uk
Animesh Jha: Institute for Materials Research, Houldsworth Building, University of Leeds, Leeds LS2 9JT, UK
Abhishek Lahiri: Institute of Electrochemistry, Clausthal University of Technology, 38678 Clausthal-Zellerfeld, Germany

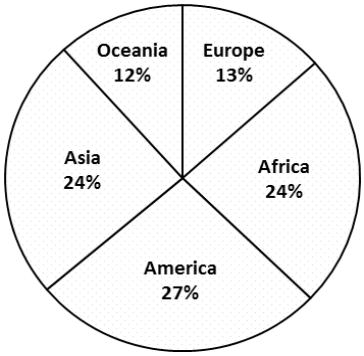

Figure 1: Ilmenite ore processing worldwide in 2011 [3], with the American continent being the single largest source .

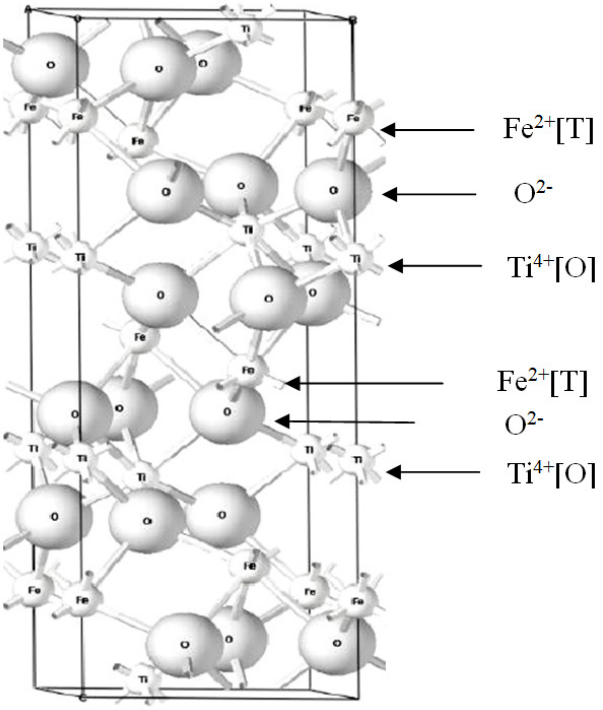

Figure 2: Ilmenite crystalline structure [O]: Octahedral site, [T]: Tetrahedral site.

Jha *et al.* [7] for the roasting of ilmenite with soda-ash, in which a two-step mechanism during the roasting process was identified. The first step involves the formation of sodium titanate as an iron depleted layer, which recedes inside by forming sodium iron titanate as an inner layer in contact with the unreacted ilmenite kernel. As the reaction progresses in air with alkali, further complexing of the product layers leads to decomposition into sodium ferrite and sodium iron titanate. In aqueous media, the sodium iron titanate dissociates into rutile (TiO_2) and sodium ferrite dissolves into water, in which Fe^{3+} must be reduced to Fe^{2+} to avoid the re-precipitation of ilmenite.

There are several reports on the carbothermic reduction of ilmenite in inert atmosphere at high temperature. However the formation of finely distributed iron, Ti_3O_5/Ti_2O_3 and iron carbide exasperates the physico-chemical separation of titanium dioxide from the iron-rich matrix. Moreover, the presence of rare-earth and zircon impurities decreases the reduction degree [8,9] of iron oxide.

Liu *et al.* [10] studied the decomposition of ilmenite with KOH solutions at 200°C at atmospheric pressure for 4 hours for achieving titanium extraction, which was limited to 85% extraction efficiency. Amer [11] carried out similar studies using NaOH at 200°C for 2 hours under 6 bar oxygen pressure, yielding a TiO_2 extraction higher than 95%. The ilmenite processing with 70% KOH solution at 100°C and further leaching with oxalic acid was presented as an efficient method to produce 98% pure anatase [12].

Ilmenite acid leaching in reducing media has been successfully tested for the extraction of 90% synthetic rutile by the addition of reducing agents like iron powder, sulfur dioxide or Ti^{3+} ions. The addition of iron powder reduces the soluble Fe^{3+} and Ti^{4+} to Fe^{2+} and Ti^{3+} respectively. Moreover Ti^{3+} also reduces Fe^{3+} to Fe^{2+} and it is oxidized to Ti^{4+} which hydrolyzes and precipitates leaving a rich ferrous solution [13]. Zhang and Nicol, 2010 [14] reported that sulfur dioxide was an efficient reductant only when Ti^{3+} ions are in the leaching media.

The aim of this work is to investigate the physico-chemical changes occurred during the alkali roasting of the non-magnetic fraction of Bomar ilmenite, which is attacked with different types of alkali salts. Following roasting a two-step leaching process is carried out for concentrating and recovering the rare earth oxide fraction and TiO_2 rich phases.

2 Experimental procedure

2.1 Mineral ore

Bomar ilmenite was selected due to its high content of rare-earth oxides. The concentrate was magnetically separated into two fractions, and the chemical compositions of both fractions were determined by X-Ray fluorescence (XRF). These results are shown in Table 1.

Table 1: Chemical compositions of the magnetic and non magnetic fractions of Bomar ilmenite.

Oxides composition	Magnetic fraction (%w/w)	Non magnetic fraction (%w/w)
TiO_2	61	75.6
FeO	28.4	0.1
Fe_2O_3	8.4	15.5
Al_2O_3	0.5	1.2
MgO	0.2	0.4
Mn_3O_4	0.2	0.3
CaO	0.1	2.1
SiO_2	1.2	2.2
P_2O_5	0.7	0.9
Cr_2O_3	0.2	0.2
CeO_2	0.2	0.9
La_2O_3	0.0	0.3

2.2 Alkali roasting

The non-magnetic fraction of the ilmenite concentrate was mixed thoroughly with the stoichometric amount of sodium, potassium and lithium carbonates and hydroxides (with analytical grade purity), explained below in Eqs. 1-6. The mixture of alkali with non-magnetic ilmenite was pressed into pellets of 2 g, using a pressure of 0.45 GPa. Each of these pellets were roasted in air at a temperature several degrees higher than the melting point of each alkali salt for 4 hours. The phases present in the roasted samples were identified by X-ray powder diffraction (XRPD) using a Bruker D8 machine with Cu-K_α radiation. Samples were scanned from 10 to 100 degrees, using a step size of 0.025 degrees and 0.75 degrees per second scan speed. The powder diffraction phase identification was carried out using X'pert high score software, which also has the JCPDS data base for comparison and identification. Roasted and leached samples were also analyzed by scanning electron microscopy (SEM-EDX), for which a part of each reacted pellet after roasting and X-ray powder diffraction analysis was mounted in Bakelite resin, polished with 0.5 μm polishing paper, carbon coated and conducted with silver paint to minimize charging during examination.

2.3 Leaching experiments

30 g of alkali roasted ilmenite in air at 900°C were used for leaching tests which were carried out in two steps - the first one was with water at room temperature for 1 hour, followed by a mixture of oxalic acid 0.3 M and ascorbic acid 0.01 M for 5 hours at 70°C in a reactor with 900 mL working volume. During leaching the stirring speed was maintained at 500 r.p.m. Elements in solution were analyzed by atomic absorption spectroscopy (AAS).

3 Results and discussion

3.1 Characterization of bomar ilmenite

The ilmenite mineral concentrate was divided into two fractions after magnetic separation yielding 53% w/w and 47% w/w, magnetic and non magnetic fractions respectively. The chemical analysis using XRF was performed on both fractions and is compared in Table 1.

Both fractions were also analyzed by SEM/EDX and XRPD techniques, for which the data are shown in Figs. 3 and 4, respectively.

The magnetic fraction is mainly composed of ilmenite, as can be deduced from the high Fe^{2+} content shown in Table 1, associated with the presence of ilmenite in Fig. 4. Iron(III) oxide was not identified in the powder diffraction patterns, which might suggest that it might be present as a solid solution in pseudorutile ($Fe_2Ti_3O_9$) and complex silicates ($K_{0.3}(Fe,Mg,Al,Ti)_{0.5}(Al,Si)_2O_6$). The non magnetic fraction is composed of rutile, pseudorutile having monazite (Ce, La, Nd) PO_4 as a secondary phase. The rare-earth rich phases do not appear in the X-ray powder diffraction pattern, because of their small volume/weight fraction in the non-magnetic fraction. The chemical and microstructural analysis confirmed that it is the non-magnetic fraction which may be worth investigating for the analysis of separation process of rare-earth oxide mixture from the remaining ilmenite matrix.

3.2 Alkali Roasting

3.2.1 Thermodynamic considerations

The computed values of Gibbs energy changes for reactions 1 to 6 are compared in Fig. 5 for the roasting condition of ilmenite with different alkali salts, using HSC 5.1 software [15]:

$$12\,KOH + 4\,FeTiO_3 + O_2\,(g) \rightarrow \rightarrow 4\,K_2TiO_3 + 4\,KFeO_2 + 6\,H_2O\,(g) \quad (1)$$

$$6\,K_2CO_3 + 4\,FeTiO_3 + O_2\,(g) \rightarrow \rightarrow 4\,K_2TiO_3 + 4\,KFeO_2 + 6\,CO_2\,(g) \quad (2)$$

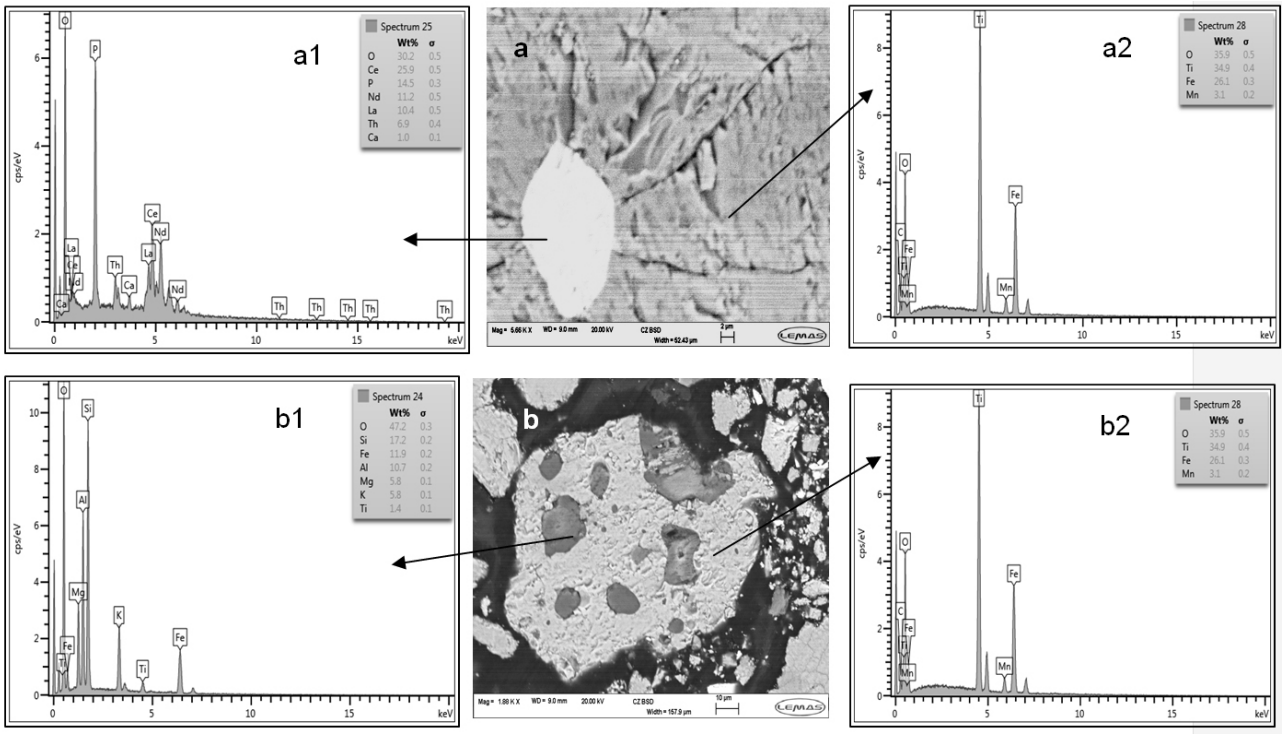

Figure 3: (a) Backscattered images of non magnetic particle of Bomar ilmenite. (a1) EDX of a monazite ((Ce, Nd, La) PO_4) inclusion. (a2) EDX of the main ilmenite ($FeTiO_3$) matrix. (b) Backscattered image of magnetic particle of Bomar ilmenite. (b1) EDX of a complex iron aluminum silicate inclusion. (b2) EDX of the main ilmenite ($FeTiO_3$) matrix.

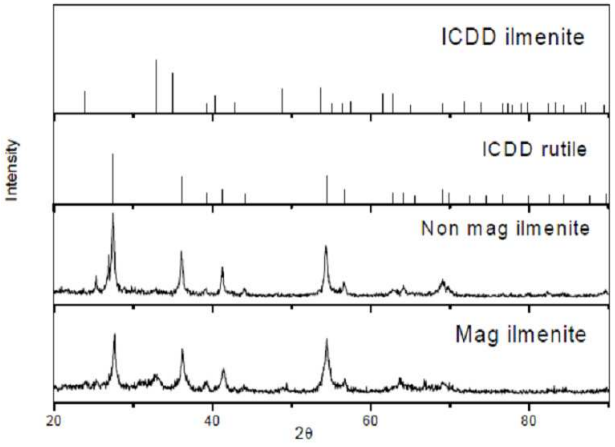

Figure 4: XRPD patterns comparison of the magnetic and non magnetic fractions of Bomar ilmenite.

$$12\,NaOH + 4\,FeTiO_3 + O_2\,(g) \rightarrow \rightarrow 4\,Na_2TiO_3 + 2\,Na_2Fe_2O_4 + 6\,H_2O\,(g) \quad (3)$$

$$6\,Na_2CO_3 + 4\,FeTiO_3 + O_2\,(g) \rightarrow \rightarrow 4\,Na_2TiO_3 + 2\,Na_2Fe_2O_4 + 6\,CO_2\,(g) \quad (4)$$

$$12\,LiOH + 4\,FeTiO_3 + O_2\,(g) \rightarrow \rightarrow 4\,Li_2TiO_3 + 2\,Li_2Fe_2O_4 + 6\,H_2O\,(g) \quad (5)$$

$$6\,Li_2CO_3 + 4\,FeTiO_3 + O_2\,(g) \rightarrow \rightarrow 4\,Li_2TiO_3 + 2\,Li_2Fe_2O_4 + 6\,CO_2\,(g) \quad (6)$$

From the Gibbs energy plots, it can be observed that the potassium based alkali salts have the largest negative values, compared to Li and Na-based alkali salts. Also the hydroxides have much larger negative values of Gibbs energy than the carbonates, which appear to be consistent with the reaction analysis for chromite based reactions reported elsewhere [16,17].

3.2.2 Sodium salts

The phase, microstructural, and morphological analyses of reaction products after alkali roasting are compared for sodium, lithium and potassium salts in Figs. 6, 7 and 8, respectively. Common features in the figures are the presence of the product layer, their structural integrity depending on the type of alkali salt used for roasting and the presence of complex titanate salts in the X-ray powder diffraction patterns.

The main phases observed using the powder diffraction technique in Fig. 6a are sodium titanate and a solid solution

of sodium ferrite and sodium aluminate. Furthermore from the SEM images in Figs. 6b and 6c, there does not seem to be any apparent evidence for the $Na_2(FeAl)_{0.5}O_2$ phase. In addition, the morphological features point to the differences in the product morphology when comparing NaOH with Na_2CO_3, suggesting that the NaOH based roasting leads to much larger scale structural changes, as apparent from extensive cracking in Fig. 6b, when compared to a limited change in the peripheral region with Na_2CO_3 in Fig. 6c. In Fig. 6c, the unreacted ilmenite kernel remains intact, showing that the ion-diffusion barrier might be much slower than that with NaOH.

In the sodium hydroxide case (Fig. 6b), the presence of intergranular cracks, minimize the diffusional limitations. These cracks are likely to be produced due to the huge difference in partial pressure values for water and carbon dioxide, being higher for water than for carbon dioxide at the same temperature [18]. It should be noted that the lattice parameter differences between ilmenite, sodium titanate, and sodium iron titanate are also significant for causing larger molar volume change, leading to cracking.

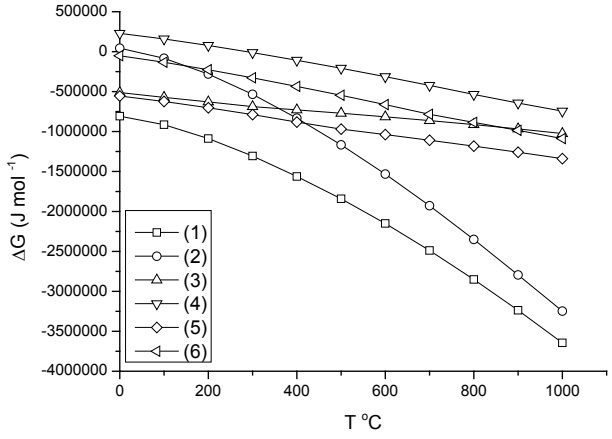

Figure 5: A comparison of the computed values of Gibbs energy (ΔG^o, J mol^{-1}) against temperature (T, °C) for the roasting of ilmenite with different alkali salts , using the HSC 5.1 software [15].

3.2.3 Lithium salts

When LiOH is used for the roasting of ilmenite, the XRPD analysis (Fig. 7a) shows the formation of a solid solution of lithium titanate and lithium ferrite, which are confirmed. However, the Li^+ ions cannot be detected in SEM due to their small electron cross-section. Also note that Li^+(0.68 Å) is much smaller than Fe^{2+}(0.74 Å) and other alkali, namely Na^+(0.97 Å) and K^+(1.33 Å), which implies

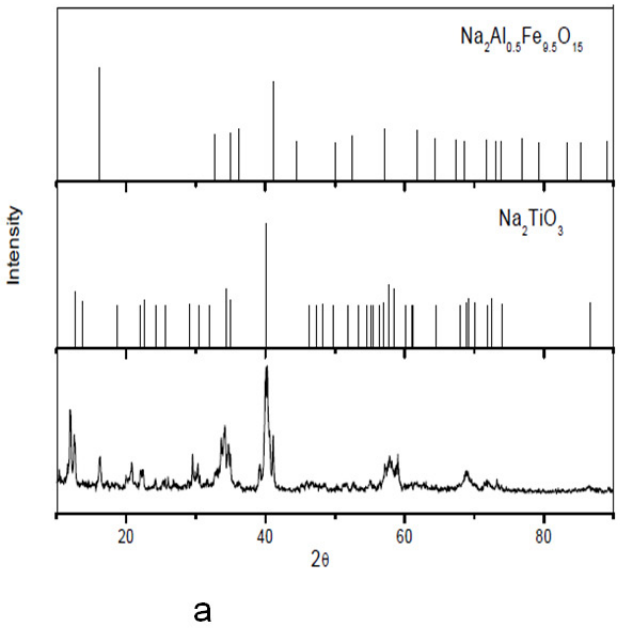

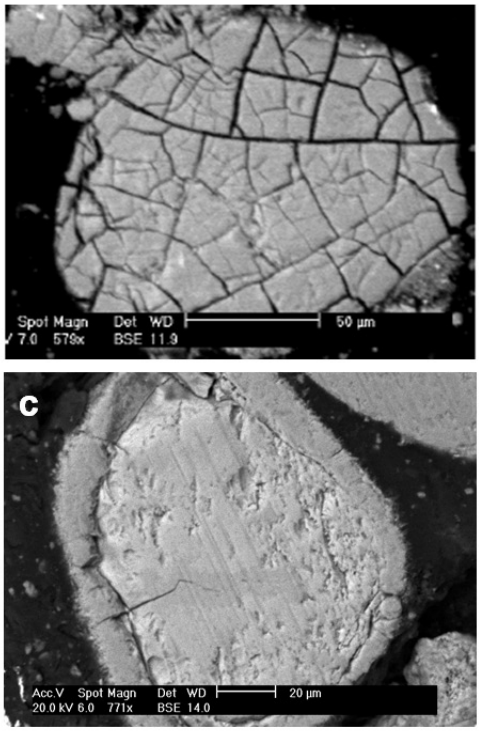

Figure 6: (a) XRPD pattern of ilmenite roasted with NaOH and Na_2CO_3; (b) backscattered image of ilmenite roasted with NaOH at 400°C; (c) backscattered image of ilmenite roasted with Na_2CO_3 at 900°C.

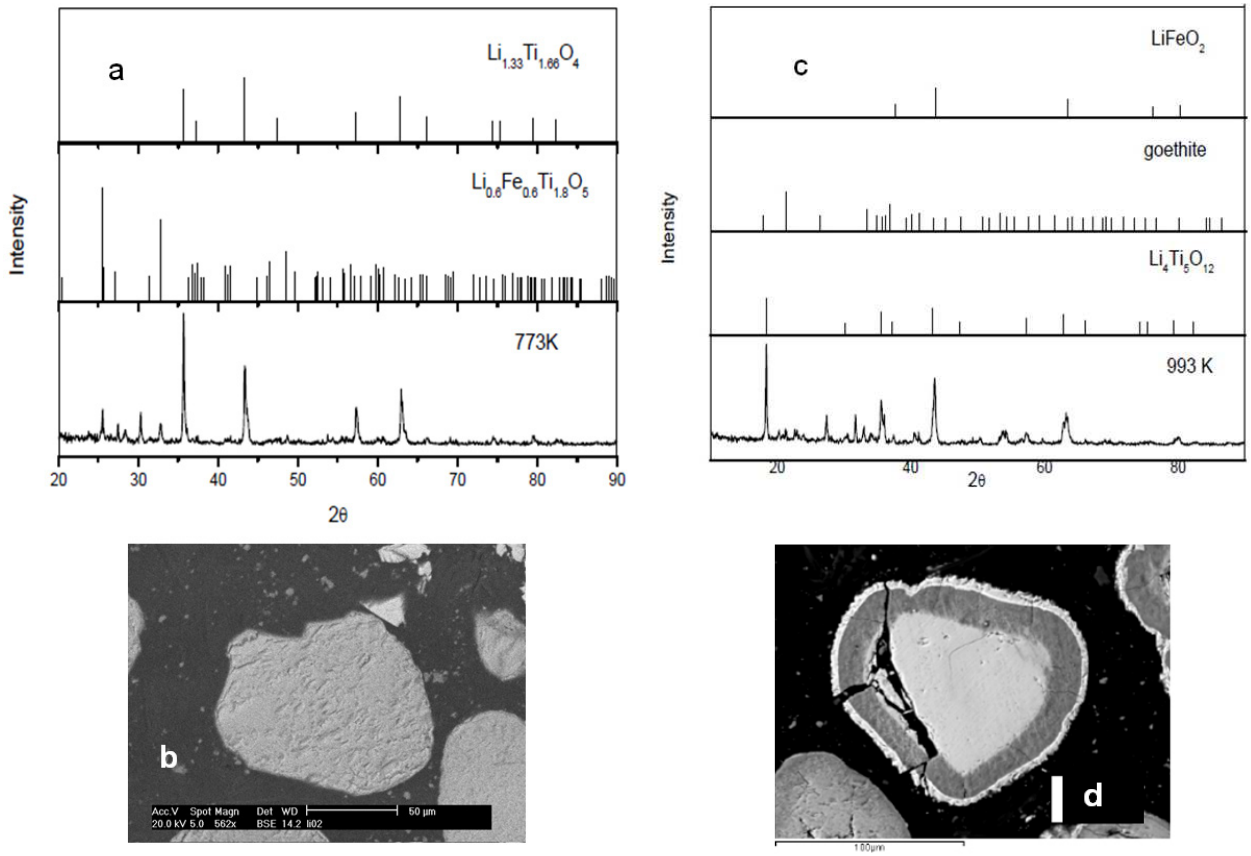

Figure 7: (a) XRPD pattern of ilmenite roasted with LiOH; (b) Backscattered image of ilmenite roasted with LiOH at 500°C; (c) XRPD pattern of ilmenite roasted with Li_2CO_3; (d) Backscattered image of ilmenite roasted with Li_2CO_3 at 700°C.

that the relative barrier for the diffusion of Li^+ in the ilmenite lattice requires much lower energy than that for Na^+ and K^+. The appearance of a homogeneous structure in Fig. 7b is an indirect evidence of the apparent solid-state ionic diffusion, in which Fe^{2+} exchanges with Li^+ in the crystalline lattice of titanate.

A layered microstructure by contrast forms showing the outermost rich lithium-iron ferrite layer, followed by complex lithium-iron-titanate, and the inner kernel of unreacted ilmenite in Fig. 7d. The XRPD patterns in Fig. 7a demonstrate these complexes together with some goethite, ferrihydrite, and $LiFeO_2$ when ilmenite was reacted with lithium carbonate at 700°C.

3.2.4 Potassium salts

Potassium salts show similar behavior to sodium ones, with the main difference in phases identified were potassium titanate and potassium ferrite. No ternary complex, potassium-iron-titanate was identified in the diffraction pattern. A major difference in the morphological feature was extensive cracking of the product layer, not only due to the partial pressure difference in the released CO_2 and H_2O, but also the ionic diffusion of K+ ions in the ilmenite lattice causing a much larger change in molar volume than that is possible either with Na or Li.

3.3. Leaching of Bomar ilmenite.

The leaching of the roasted ilmenite with carbonates was performed in two steps. In the first step with water, the alkali ferrites were solubilized from the reacted solid mass into the solution. The percentage of iron removal with different alkali carbonates is shown in Table 2. The filtered solid was rich in alkali-iron titanate, which remain insoluble and settles under gravity.

Table 2 shows that the iron removal is fractionally higher for potassium than sodium carbonate, with no removal observed in the case of lithium carbonate, since lithium ferrite is insoluble in water [19].

Another interesting observation was the formation of a colloidal layer on the top of the reactor. This layer was filtered and analyzed using XRF with the chemical composition listed in Table 3.

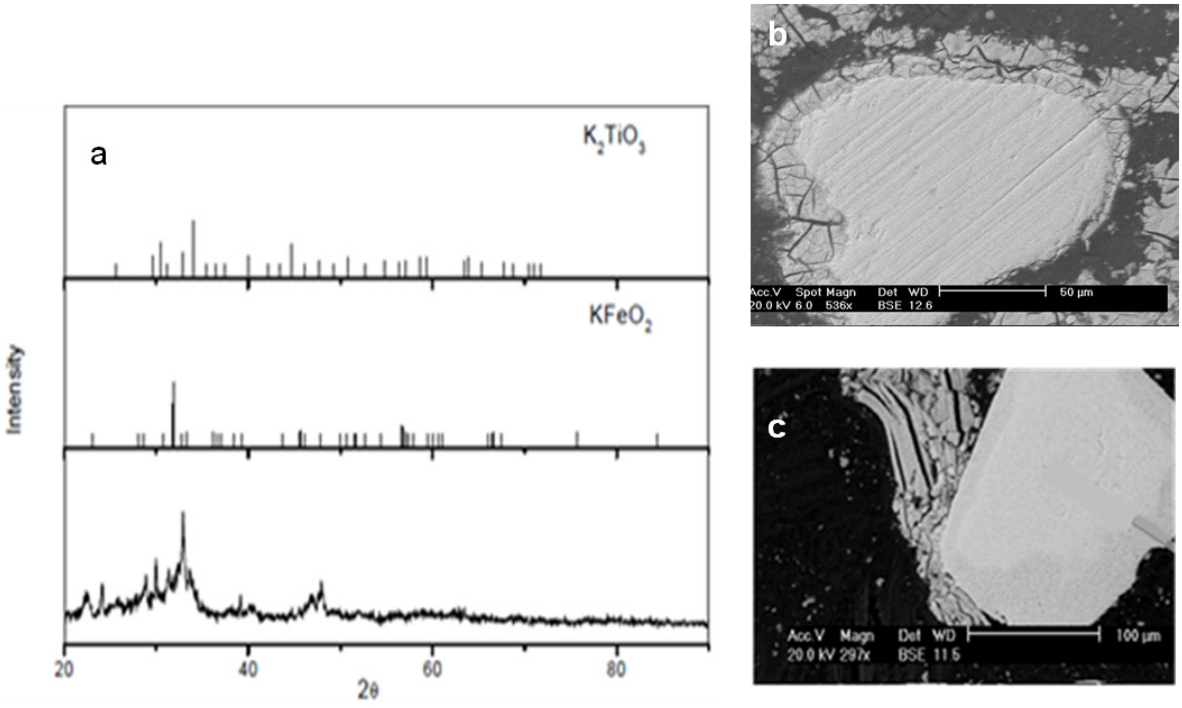

Figure 8: (a) XRPD pattern of ilmenite roasted with KOH and K_2CO_3; (b) Backscattered image of ilmenite roasted with KOH at 500°C; (c) Back scattered image of ilmenite roasted with K_2CO_3 at 900°C.

Table 2: Iron removal percentage after water leaching of ilmenite with alkali carbonates

Alkali carbonate	Iron removal (%)
Na_2CO_3	43
Li_2CO_3	0
K_2CO_3	47

Table 3: Chemical composition of the colloidal layer during the water leaching of Bomar ilmenite roasted with K_2CO_3 and Na_2CO_3

Elements	Concentration (%w/w)
Ca	69.8
La	5.72
Ce	5.35
Si	5.05
Th	3.82
Nd	2.97
Pr	1.86
P	1.72
Y	0.64
Fe	0.53
Mg	0.36
Sm	0.13
Al	0.12

The results in Table 3 show that the alkali roasting treatment yields a concentrate rich in rare earth oxides, which can be recovered. Total rare earth elements analyzed was around 16-17%wt, from both sodium and potassium alkali roasting. The observation of colloidal suspension after leaching the roasted mass was conspicuously absent when the lithium salt was used for roasting, which suggests that the morphological change in the form of extensive cracking in the mineral matrix shown in Figs. 6 and 8 is the root cause for the physical liberation of fine rare-earth oxide particles. In the alkali medium the rare-earth particulates have residual like charge which keeps individual particles apart, favouring the formation of colloidal layer.

During the leaching process a pH increase was observed due to the following reactions:

$$5\,Na_2TiO_3 + H_2O \rightarrow Na_8Ti_5O_{14} + 2\,NaOH \quad (7)$$

$$Na_2Fe_2O_4 + H_2O \rightarrow Fe_2O_3 + 2\,NaOH \quad (8)$$

$$Fe_2O_3 + 3H_2O \rightarrow 2\,Fe(OH)_3 \quad (9)$$

In these reactions sodium hydroxide is released and the soluble sodium ferrite dissociates into iron(III) oxide according to Reaction 8. The sodium hydroxide released

reacts with bubbling carbon dioxide into the solution and regenerates sodium carbonate which can be recycled and used in the roasting process.

The second leaching step was carried out using a mixture of oxalic and ascorbic acid, with the aim to remove the remaining iron present in the alkali titanates, as shown in the powder diffraction patterns in Figs. 6 and 8. This is consistent with the E_H-pH diagram reported earlier by Jha and co-workers [7,20]. For iron removal, the pH must be buffered below 4, so that Fe^{3+} reduces to Fe^{2+} and remains in solution under acidic condition in the absence of oxidizing atmosphere. Suter *et al.* [21], reported the reduction of Fe^{3+} to Fe^{2+} by ascorbic acid according to the following scheme:

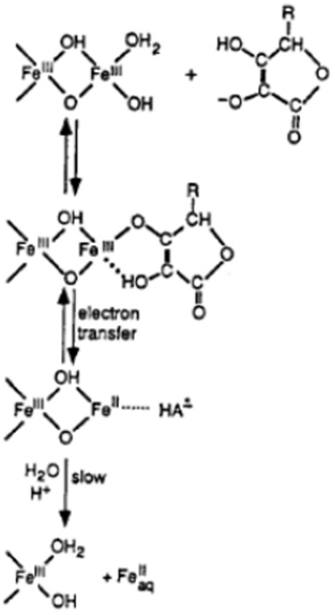

Figure 9: Reduction mechanism of iron(III) hydroxide to produce iron (II) ions [21].

Once Fe^{+2} ions are produced they solubilize in the leaching media and react with oxalic as well as sodium titanate to produce iron oxalate and rutile respectively *via* Reactions 10 and 11.

$$Fe(OH)_2 + H_2C_2O_4 \rightarrow FeC_2O_4 + 2H_2O \quad (10)$$

$$Na_8Ti_5O_{14} + 4\,H_2C_2O_4 \rightarrow 5\,TiO_2 + 4\,Na_2C_2O_4 + 4\,H_2O \quad (11)$$

After five hours leaching the solid waste was analyzed with the results are shown in Fig. 10 and Table 4.

From Fig. 10 and Table 4 we can see that the leached product has a high content of titanium in the form of rutile and anatase. During the leaching sodium titanate and ferrite decomposes according to Reactions 7-11, which is apparent from the evidences presented in the X-Ray powder diffraction pattern of the leached samples.

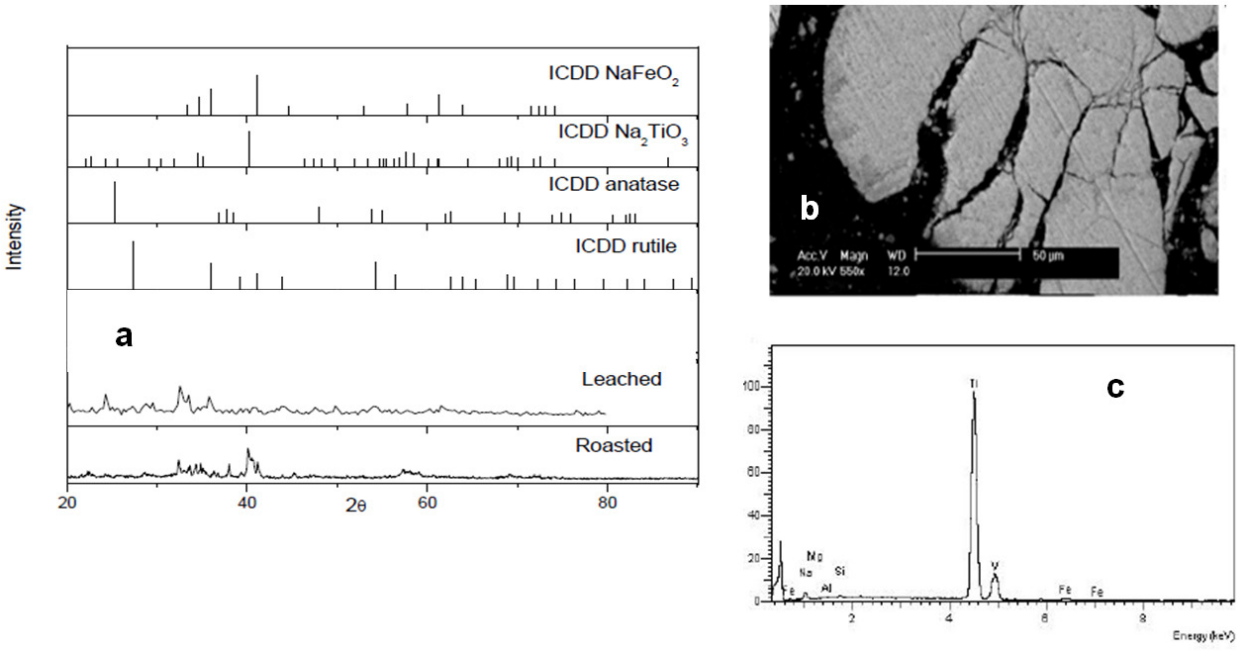

Figure 10: (a) XRPD pattern of organic acids leaching waste; (b) Backscattered image of organic acids leaching waste; (c) EDX of organic acids leaching waste.

Table 4: Chemical composition comparison of the non-magnetic fraction of the Bomar ilmenite and the leached product after organic acids leaching.

Chemical composition (%w/w)		
Compounds	**Non magnetic fraction**	**Leached product**
TiO_2	75.6	97.0
FeO	0.1	0.0
Fe_2O_3	15.5	1.3
CeO_2	0.9	0.0
La_2O_3	0.3	0.0

4 Conclusions

1. The alkali roasting is a novel route for controlling the separation of major and minor elements presented in the Bomar ilmenite.
2. Rare earth oxides are not attacked by alkali salts during the roasting and are physically liberated from the mineral lattice.
3. Lithium salts form a compact structure after the roasting stopping liberation of the rare earth oxides and removal of iron to produce synthetic rutile.
4. There is potential for the recovery of the alkali released during the aqueous leaching steps by carbon dioxide bubbling, which reduces atmospheric emissions and enhances process economy.
5. The leaching of the product with a mixture of oxalic and ascorbic acid allows helps the precipitation synthetic rutile with a purity of 97% w/w.

Acknowledgements: A. Jha wishes to thank the Marie Curie Intra European Fellowship in the Framework Programme 7 of the EU Community Framework Programme for the award of fellowship to Dr S. Sanchez-Segado. The authors also acknowledge the support from Mr M. Javed and Mr S. R. Lloyd during this project.

References

[1] Habashi F., Handbook of Extractive Metallurgy, Wiley-VCH, New York, 1997, Vol.3
[2] Chen X., Mao S.S., Chem. Rev., 2007, 107
[3] Brown T.J. et al., World mineral production, British Geological Survey, Nottingham, 2013
[4] Kingery W.D. et al., Introduction to ceramics, 2nd ed., Wiley-Interscience, New York, 1981
[5] Lahiri A., Jha A., Metall. Mater. Trans. B, 2007, 38
[6] Foley E. et al., J. Solid State Chem., 1970, 1
[7] Jha A. et al., Metall. Mater. Trans. C, 2008, 117
[8] Wang Y., Yuan Z., Int. J. Miner. Process, 2006, 81
[9] Wang Y. et al., Trans. Nonferrous Met. Soc. China, 2008, 18
[10] Liu Y. et al., Int. J. Miner. Process, 2006, 81
[11] Amer A.M, Hydrometallurgy, 2002, 67
[12] Nayl A.A., Aly H.F., Hydrometallurgy, 2009, 97
[13] Mahmoud M.H.H. et al., Hydrometallurgy, 2004, 73
[14] Zhang S., Nicol M.J., Hydrometallurgy, 2010, 103
[15] Roine A., Outokumpu HSC Chemistry for Windows User´s guide, version 5.1, 2002
[16] Sanchez-Segado S., Jha A., TMS Annual Meeting, 2013
[17] Tathavadkar V.D., Antony M.P., Jha A., Metall. Mater. Trans. B, 2005, 36
[18] Poling B.E. et al., The properties of gases and liquids, 5th ed., Mc Graw Hill, New York, 2001
[19] Barriga C. et al., J. Solid State Chem., 1988, 77
[20] Lahiri A., Jha A., Hydrometallurgy, 2009, 95
[21] Sutter D. et al., Langmuir, 1991, 7(4)